

# EndoUFM: Utilizing Foundation Models for Monocular depth estimation of endoscopic images

Xinning Yao<sup>1</sup>, Bo Liu<sup>1,2</sup>, Bojian Li<sup>1</sup>, Jingjing Wang<sup>1</sup>, Jinghua Yue<sup>1</sup>, and Fugen Zhou<sup>1</sup>

**Abstract**—Depth estimation is a foundational component for 3D reconstruction in minimally invasive endoscopic surgeries. However, existing monocular depth estimation techniques often exhibit limited performance to the varying illumination and complex textures of the surgical environment. While powerful visual foundation models offer a promising solution, their training on natural images leads to significant domain adaptability limitations and semantic perception deficiencies when applied to endoscopy. In this study, we introduce EndoUFM, an unsupervised monocular depth estimation framework that innovatively integrating dual foundation models for surgical scenes, which enhance the depth estimation performance by leveraging the powerful pre-learned priors. The framework features a novel adaptive fine-tuning strategy that incorporates Random Vector Low-Rank Adaptation (RVLRA) to enhance model adaptability, and a Residual block based on Depthwise Separable Convolution (Res-DSC) to improve the capture of fine-grained local features. Furthermore, we design a mask-guided smoothness loss to enforce depth consistency within anatomical tissue structures. Extensive experiments on the SCARED, Hamlyn, SERV-CT, and EndoNeRF datasets confirm that our method achieves state-of-the-art performance while maintaining an efficient model size. This work contributes to augmenting surgeons’ spatial perception during minimally invasive procedures, thereby enhancing surgical precision and safety, with crucial implications for augmented reality and navigation systems.

## I. INTRODUCTION

Minimally Invasive Surgery (MIS) has revolutionized modern medicine, offering patients smaller incisions and quicker recovery times. To further advance surgical precision and safety, the field is increasingly turning to robotic systems enhanced with augmented reality (AR) [1], [2]. A cornerstone of these AR applications is the ability to generate a real-time 3D reconstruction of the surgical site, which fundamentally relies on accurate depth estimation. Given the challenges in obtaining ground-truth data from inside the body and the widespread use of single-camera endoscopes, unsupervised monocular depth estimation (UMDE) has emerged as a particularly flexible and practical area of research [3], [4].

However, the endoscopic environment presents a formidable challenge for existing depth estimation techniques. The confined surgical cavity is subject to dynamic and complex conditions, including non-uniform illumination, intense specular reflections off tissue surfaces,

This work was supported in part by the Beijing Natural Science Foundation (L232037, L242112, L222034, L252005, and L222104).

<sup>1</sup>Image Processing Center, Beihang University, Beijing, 100191, China.  
<sup>2</sup>State Key Laboratory of High-Efficiency Reusable Aerospace Transportation Technology, Beijing 102206, China. Corresponding Author: bo.liu@buaa.edu.cn



Fig. 1. Left: single frame image from MIS scenes. Middle: depth estimation result from Depth Anything Model [5]. Right: depth estimation result from our method EndoUFM. EndoUFM can accurately estimate the depth of surgical instruments and, compared with Depth Anything Model, better perceive the anatomical structures behind the instruments. It maintains depth consistency within tissues even in challenging scenarios involving specular reflections, instrument occlusions, and complex tissue structures.

tissue deformation, and frequent occlusions by surgical tools. These factors severely undermine traditional UMDE methods, which often rely on photometric consistency and rigid scene assumptions that do not hold up in a live surgical setting [6], [7], [8]. While some strategies have been developed to address these issues, such as modeling illumination changes [9] or using intrinsic image decomposition [7], they still struggle with the drastic lighting shifts and limited global perception inherent in traditional Convolutional Neural Network (CNN) architectures. Moreover, self-supervised learning methods often do not generalize well to other anatomies and patients, while the scale and reliable transfer learning capabilities of foundation models show promise to overcome these limitations [10].

The recent advent of large-scale visual foundation models offers a powerful new path forward. Models like Depth Anything [5], pre-trained on millions of diverse natural images, have learned robust geometric priors that are invaluable for understanding 3D space. Similarly, medical-specific models like MedSAM [11], an adaptation of the Segment Anything Model, excel at identifying and outlining the complex anatomical structures found in medical imagery. By harnessing these powerful, pre-learned priors, it is possible to dramatically improve depth estimation in the difficult endoscopic domain.

Yet, these powerful models cannot be applied directly off the shelf, as shown in Fig. 1. Firstly, the way of integrating the foundation models with the UMDE framework needs to be studied to achieve the better use of the capacity of the foundation models [10]. Secondly, their training on general or natural images results in a significant domain gap, leading to “domain adaptability limitations and semantic perception deficiencies” when confronted with unique endoscopic video data. While parameter-efficient fine-tuning methods like Low-Rank Adaptation (LoRA) [12] can help adapt

these large models to new tasks, they can lack robustness and fail to adequately capture local, fine-grained details in endoscopic scenes.

To address these challenges, we propose EndoUFM, a novel unsupervised monocular depth estimation framework that synergistically integrates dual foundation models—DepthAnything for robust depth prediction and the Segment Anything Model (SAM) for detailed image decomposition. EndoUFM leverages their pre-learned priors to enhance depth estimation accuracy and semantic coherence in endoscopic scenes. Recognizing the difficulty of adapting foundation models to the unique endoscopic domain, we introduce a sophisticated adaptive fine-tuning strategy featuring Random Vector Low-Rank Adaptation (RVLORA), which enhances model adaptability without significantly increasing trainable parameters. Additionally, we incorporate Residual blocks based on Depthwise Separable Convolution (Res-DSC) to capture fine-grained local features essential for precise depth prediction. To further ensure semantic consistency, we design a mask-guided smoothness loss that enforces depth consistency within anatomical tissue structures using SAM-derived segmentation masks. Extensive experiments on the SCARED, Hamlyn, SERV-CT, and EndoNeRF datasets demonstrate that EndoUFM achieves state-of-the-art performance, surpassing existing methods in robustness and accuracy. By enhancing surgeons' spatial perception, EndoUFM holds transformative potential for improving AR and navigation systems in MIS, thereby advancing surgical precision and safety.

This work is an extensive extension of our preliminary work reported in International Conference on Intelligent Robots and Systems (IROS). The enhancements include the synergistic integration of dual foundation models to the UDME framework, the foundation model-enhanced loss, and more thorough validations on more datasets. In summary, our main contributions are:

- We pioneer EndoUFM, a new unified framework that represents a novel paradigm of fusing dual foundation models to adapt large-scale vision knowledge for specialized endoscopic applications.
- We propose an adaptive fine-tuning strategy, incorporating our novel RVLORA and Res-DSC modules, to efficiently adapt foundation models to the unique challenges of endoscopic depth estimation.
- We design the foundation model-enhanced loss, leveraging the pre-segmented masks generated from foundation models to reduce semantic ambiguity in depth predictions.
- We demonstrate through extensive experiments on four public datasets that our method achieves state-of-the-art performance and superior robustness, all while maintaining an efficient model size suitable for real-world clinical deployment.

## II. RELATED WORKS

### A. *Unsupervised monocular depth estimation based on CNN*

UMDE has seen significant advancements in natural image domains. Early work by Zhou et al. [4] pioneered the use of view synthesis for UMDE. This was further enhanced by Godard et al. [8], who improved performance through per-pixel loss minimization and automatic masking techniques. Despite these breakthroughs in natural scenes, most of these methods rely on the assumption of photometric consistency. This reliance severely limits their effectiveness in endoscopic environments, which are characterized by highly variable illumination. To mitigate this issue, researchers have explored various strategies. For instance, Ozyoruk et al. [6] and Shao et al. [9] first pre-processed images to adjust lighting before performing depth estimation. Another approach, proposed by Li et al. [7], improved results by employing intrinsic image decomposition to separate illumination variations and then leveraging reflectance consistency. Wang et al. [13] introduced MonoPCC, a novel approach that fundamentally resolves brightness variations by reforming the photometric constraint into a cycle-consistent warping mechanism. Beyond these photometric consistency-based methods, Battile et al. [14] utilized a photometric stereo technique for depth estimation in the human colon. Despite these advancements, existing methods often lack global scene understanding and struggle with the unique characteristics of endoscopic images.

### B. *The Application of Foundation Models in Depth Estimation*

In recent years, foundation models for depth estimation have begun to show immense potential. Compared to conventional CNNs, Vision Transformer(ViT)-based architectures of foundation models offer stronger global context modeling, effectively alleviating the limitations of local receptive fields. Ranftl et al. [15] introduced MiDaS to improve the model's generalization ability across different scenes by aligning the scale and shift of depth maps and mixing datasets with different annotations during training. Oquab et al. [16] proposed DINOv2, a powerful visual representation foundation model that has shown outstanding performance in a wide range of computer vision tasks, including depth estimation. More recently, Depth Anything [5] trained a depth estimation foundation model using larger-scale labeled and unlabeled datasets and designed an auxiliary supervision to enable the model to inherit rich semantic priors from the pre-trained DINOv2 encoder. In the medical domain, the first foundation model specifically for zero-shot cross-dataset depth estimation in endoscopy was proposed by Tian et al. [17] with their work, EndoOmni. The model is characterized by a robust self-learning framework with a teacher-student model that learns from a mix of labeled and unlabeled data. However, due to the limited data in the medical field, it remains challenging to train and build medical-specific foundation models from scratch. Therefore, adopting general-purpose foundation models for specific task domains is a practical

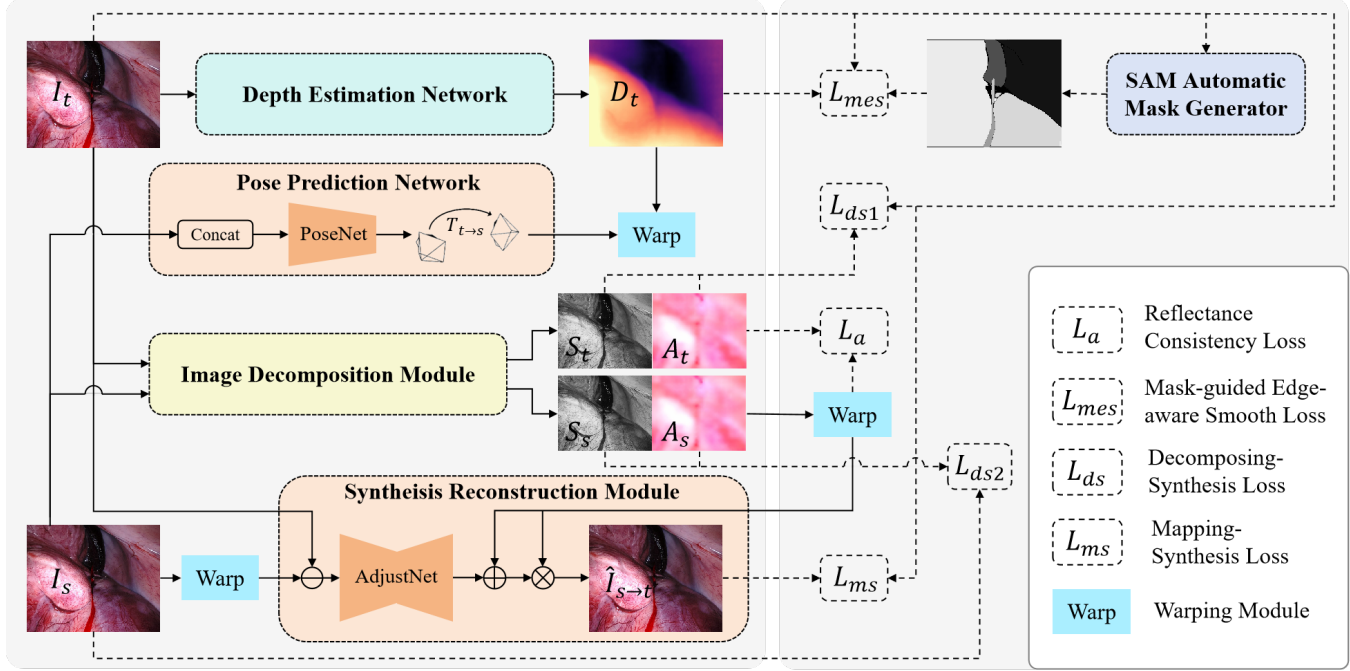


Fig. 2. Network architecture.

and effective strategy. In endoscopic depth estimation, Cui et al. [18] first proposed Surgical-DINO, which utilizes the DINOv2 encoder for improved feature extraction. Their follow-up work, EndoDAC [19], applied Depth Anything to the depth estimation network and achieved relatively better prediction results. Yang et al. [20] proposed an innovative framework that integrates CLIP [21] with segmentation tasks to enhance encoder performance and boost depth estimation quality. Nevertheless, directly applying foundation models to endoscopic imagery still faces problems such as domain adaptation limitations and semantic perception deficiencies. How to efficiently integrate and exploit the capabilities of foundation models for robust and accurate endoscopic depth estimation remains an open research problem requiring further exploration.

### C. Low-rank adaptation

With the widespread application of large models, LoRA [12] revolutionized the efficient training of large language models for specialized tasks. Its core innovation lay in decomposing weight matrices into two low-rank components, A and B, which drastically cut down on training resource demands. This foundational concept has since inspired numerous advancements. For instance, LoRA+ [22] boosted efficiency by assigning distinct learning rates to matrices A and B. AdaLoRA [23], proposed by Zhang et al., further refined this by adaptively selecting different ranks for various adapters, thereby improving LoRA's learning capacity and training stability. VeRA [24] pushed parameter reduction even further by freezing matrices A and B and introducing auxiliary trainable vectors, though this came with a slight decline in accuracy. Given that the effectiveness of diverse fine-tuning strategies varies across different tasks,

Cui et al.[19] recently proposed DV-LoRA to efficiently adapt foundation models to surgical scene depth estimation. DV-LoRA is an initial exploration of fine-tuning methods for endoscopic scenes, improving upon the results of applying general LoRA directly to endoscopic images. Seeing the potential for improving LoRA for specific scenes, there is a clear need to further investigate a fine-tuning approach specifically tailored for endoscopic depth estimation tasks.

## III. METHOD

In this section, we present the architecture of EndoUFM, our novel framework for unsupervised monocular depth estimation. We detail the integration of foundation models, our adaptive fine-tuning strategy, and the custom loss functions that collectively enable state-of-the-art performance on endoscopic images.

### A. EndoUFM framework Integrated with Foundation Models

We propose a novel decomposition-based unsupervised monocular depth estimation framework designed to enhance robustness and accuracy in endoscopic scenarios by leveraging foundation models. Our improvement consists of two main components: a depth estimation network built on the Depth Anything Model and an image decomposition network augmented with the Segment Anything Model (SAM), specifically MedSAM. These components are designed to address the domain shift and semantic inconsistency challenges prevalent in endoscopic images.

Our proposed network, as illustrated in Fig. 2, is based on our previous work IID-SfMLearner [7]. We define the target frame as  $I_t$  and the adjacent source frames as  $I_s$ . The network comprises a depth estimation network  $\Phi_D$  for predicting single-frame depth, a pose estimation network

$\Phi_T$  to estimate the relative inter-frame camera pose  $T_{t \rightarrow s}$ , a decomposition module  $\Phi_I$  to decompose images into reflectance ( $R$ ) and shading ( $S$ ) maps, and a synthesis and reconstruction module  $\Phi_L$  to reconstruct the target frame  $\hat{I}_{s \rightarrow t}$  from the decomposed components.

Classical monocular depth estimation methods typically employ standard convolutional neural networks for depth prediction, which often lack sufficient global perception to accurately capture depth information. To improve depth prediction, we replace the conventional network with the Depth Anything transformer backbone, enabling the model to capture long-range geometric priors while retaining local anatomical details. As shown in the Fig. 3(a), the encoder and decoder maintain the same structure as the Depth Anything Model. Features from the last four encoder layers are fed into its frozen Reassemble & Fusion module, which generates and aggregates features at different resolutions. The features then pass through the trainable Depth-Head module for final dense prediction, yielding depth estimation outputs at four scales. Furthermore, we integrate the powerful architecture of the Segment Anything Model (SAM) [25] into our image decomposition network. This infusion of semantic information significantly enhances the network's awareness and decomposition capabilities in scenes with complex textures and varying illumination, overcoming the limitations of previous ResNet-based decomposition networks [7]. As shown in the Fig. 3(b), the encoder is same with the SAM's vision transformer architecture and the decoder structure is similar to that of the depth estimation network, with the Depth-Head modified to a Reflectance-Head and a Shading-Head for image decomposition. Features extracted by the SAM encoder are firstly decoded to generate the reflectance map. Then the shallow features from the decoder are concatenated with the original image to incorporate fine details, and then processed by the shading head to predict the shading map.

#### B. Adaptive Foundation Model Fine-Tuning Strategy

Fine-tuning foundation models presents a direct approach to enhance long-range dependencies without significantly increasing the number of trainable parameters. Although Depth Anything Model has been proposed for depth estimation, it is trained on natural images, leading to suboptimal performance when directly applied to endoscopic images. To address this issue, we propose a novel fine-tuning strategy specifically tailored for endoscopic images, as shown in Fig. 3(c), which integrates Random Vector Low-Rank Adaptation (RVLORA) and Residual blocks based on Depthwise Separable Convolution (Res-DSC).

1) *Low-rank Adaptation Based on Random Vectors (RVLORA):* While neural networks often contain numerous dense layers with full-rank weight matrices, pre-trained foundation models demonstrate a surprisingly low "intrinsic dimension" when adapted to specific tasks [26]. This suggests that effective learning can still occur when parameters are projected into smaller, random subspaces. Inspired by this, Low-Rank Adaptation (LoRA) was proposed [12], positing that weight updates during adaptation also exhibit a low

"intrinsic rank". For a pre-trained weight matrix  $W_0 \in \mathbb{R}^{m \times n}$ , its update can be efficiently represented through low-rank decomposition as  $W_0 + \Delta W = W_0 + BA$ . The modified forward pass then becomes:

$$h = W_0x + \Delta Wx = W_0x + BAx \quad (1)$$

where  $B \in \mathbb{R}^{m \times r}$  and  $A \in \mathbb{R}^{r \times n}$ , the rank  $r$  is significantly smaller than both  $m$  and  $n$  ( $r \ll \min(m, n)$ ). During the training process,  $W_0$  remains frozen and does not receive gradient updates. Instead, only matrices  $A$  and  $B$  are trainable. This approach injects these trainable low-rank decomposition matrices into each layer of the transformer architecture, drastically reducing the number of trainable parameters for downstream tasks while keeping the core pre-trained model weights intact.

Recent research has shed light on the surprisingly potent role of random weights in deep learning models. On one hand, the strategic introduction of random vectors can significantly boost a model's adaptive capacity. This provides an efficient mechanism for fine-tuning a model's behavior without the computational costs associated with extensive retraining or parameter adjustments [24], [27]. On the other hand, several cutting-edge deep learning techniques, particularly those focused on feature learning and transformations, heavily leverage affine transformations of learned features. It has been shown that freezing these randomly initialized parameters can actually enhance a network's innate ability to capture and generalize these affine transformations more effectively [28]. Furthermore, in the tasks of monocular depth estimation, an inherent challenge is scale ambiguity. The depth information can vary depending on the specific context and scale of the scene. The introduction of random vectors, specifically engineered for scale adjustment, can profoundly improve a model's flexibility. This allows the model to more robustly adapt to varying scales encountered during inference, leading to more consistent and accurate depth predictions.

Inspired by these insights, we propose a parameter-efficient fine-tuning method: Low-Rank Adaptation based on Random Vectors (RVLORA). RVLORA builds upon the foundational concept of LoRA but introduces a crucial enhancement: the integration of randomly initialized vectors  $a$  and  $b$ . These vectors serve to scale the low-rank matrices, thereby enhancing the model's adaptability across different scales and contexts. During the training phase, we employ Kaiming uniform initialization [29] for vectors  $a$ ,  $b$ , and the low-rank matrix  $A$ , while the low-rank matrix  $B$  is initialized to zeros. This specific initialization strategy ensures that the original weight matrix remains unaffected during the first forward pass. The frozen scaling vectors and the trainable low-rank matrices are combined with the original, pre-trained weights without causing additional inference delay. Our proposed method can be formally represented as:

$$h = W_0x + \Delta Wx = W_0x + \Lambda_b B \Lambda_a Ax \quad (2)$$

where  $B \in \mathbb{R}^{m \times r}$  and  $A \in \mathbb{R}^{r \times n}$  represent the trainable low-rank matrices, and the rank  $r$  is much smaller than

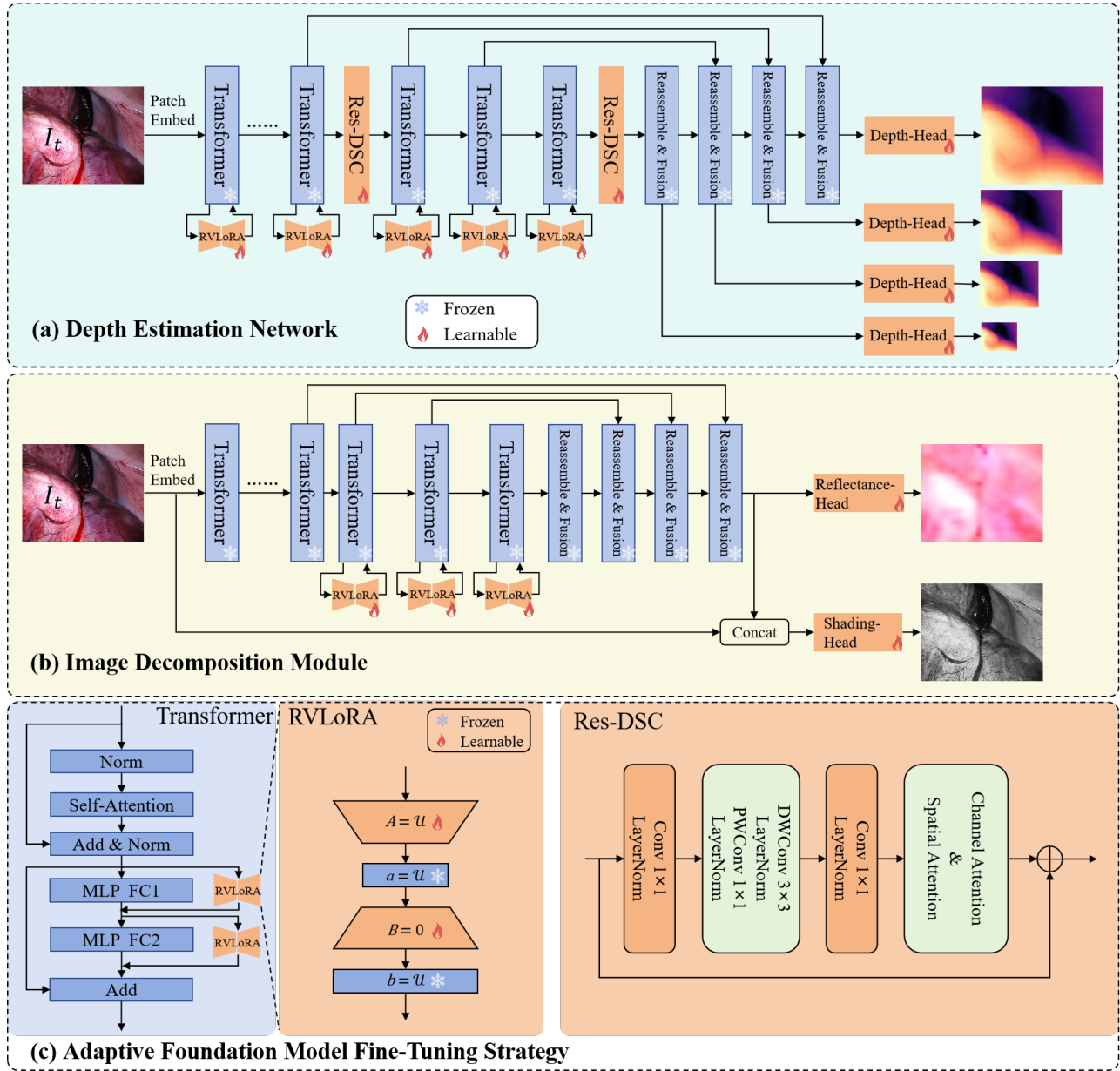


Fig. 3. (a) Depth estimation network. (b) Image Decomposition Module. (c) Adaptive Foundation Model Fine-Tuning Strategy. left: The deployment and detailed structure of RVLoRA. RVLoRA is connected to the two linear layers of the MLP in each transformer module. The parameters  $a$  and  $b$  are frozen while  $A$  and  $B$  are trainable. Bottom-right: The detailed structure of Res-DSC. Res-DSC contains a depthwise separable convolution, a pointwise separable convolution, a channel attention module, and the residual connection.

both  $m$  and  $n$  ( $r \ll \min(m, n)$ ). The novel components are  $\Lambda_b \in \mathbb{R}^{m \times m}$  and  $\Lambda_a \in \mathbb{R}^{r \times r}$ . These are diagonal matrices derived from the randomly initialized vectors  $b \in \mathbb{R}^{m \times 1}$  and  $a \in \mathbb{R}^{r \times 1}$ , respectively. Crucially,  $b$  and  $a$  are randomly initialized and then remain frozen throughout the entire training process. This approach effectively applies random scaling to the rows of the low-rank matrices  $B$  and  $A$ , which in turn enhances the model's adaptability across layers of the network.

As shown in Fig. 3(a), we apply the pre-trained Depth Anything Model and fine-tune all the transformer blocks in the encoder to specifically enhance the accuracy of depth

estimation. The SAM encoder framework we employ is detailed in Fig. 3(b). To adapt to endoscopic images, we utilized a pre-trained MedSAM model [11], allowing the model to leverage learned medical prior information. To optimize training parameters and time, we fine-tune only the bottom three transformer blocks of the encoder [30], which demonstrably improves performance.

2) *Residual Block Based on Depthwise Separable Convolution (Res-DSC)*: While transformers excel at dynamic attention, global context awareness, and generalization, they often struggle with extracting fine details and local features. Conversely, convolutions are adept at capturing local features and offer inherent benefits such as shift, scale, and distortion

invariance. Combining CNNs with Transformers can create a synergistic effect, significantly boosting overall model performance.

Inspired by this, we designed a Residual block based on Depthwise Separable Convolution (Res-DSC), as shown in Fig. 3(c). This structure utilizes three convolutional layers: an initial 1x1 convolution layer for channel reduction, a 3x3 depth-wise separable convolution, which reduces parameters for faster computation and a more streamlined model compared to traditional convolutions. A 1x1 convolution then restores the number of channels. We also incorporate channel attention and spatial attention modules [31]. By combining these, the input features are doubly refined, allowing the model to simultaneously focus on which channels and spatial locations of the features are most important.

To minimize model parameters while maintaining depth estimation accuracy, we incorporate Res-DSC blocks only after the 3rd, 6th, 9th, and 12th transformer blocks of the depth estimation network. For brevity, Fig. 3(a) only illustrates the Res-DSC blocks after the 9th and 12th transformer blocks.

### C. Foundation Model-Enhanced loss design

Similar to the loss function design of IID-SfMLearner, we first reconstruct a synthetic frame  $I_{s \rightarrow t}$  via a warping transformation using the predicted depth  $D_t$  from the depth estimation network and the relative pose  $T_{t \rightarrow s}$ . Based on the image decomposition theory [32], a reflectance consistency loss  $L_a$  is formulated to minimize the reflectance difference between adjacent frames. A decomposing-synthesis loss  $L_{ds}$  and a mapping-synthesis loss  $L_{ms}$  are also introduced to constrain the decomposition and reconstruction processes. The expressions for these three loss functions are as follows:

$$L_a(R_t, R_{s \rightarrow t}) = \|R_t - R_{s \rightarrow t}\|_1 \quad (3)$$

$$\begin{cases} L_{ds1}(\hat{I}_t, I_t) = \alpha \frac{1 - SSIM(\hat{I}_t, I_t)}{2} + (1 - \alpha) \|\hat{I}_t - I_t\|_1 \\ L_{ds2}(\hat{I}_s, I_s) = \alpha \frac{1 - SSIM(\hat{I}_s, I_s)}{2} + (1 - \alpha) \|\hat{I}_s - I_s\|_1 \end{cases} \quad (4)$$

$$L_{ms}(\hat{I}_{s \rightarrow t}, I_t) = \alpha \frac{1 - SSIM(\hat{I}_{s \rightarrow t}, I_t)}{2} + (1 - \alpha) \|\hat{I}_{s \rightarrow t} - I_t\|_1 \quad (5)$$

where  $\alpha$  is a hyperparameter to balance the L1 loss and SSIM loss, and set to 0.85 in our method.

To further leverage the capabilities of the SAM model, we utilize automatically generated segmentation masks from the pre-trained model to construct a mask-guided depth smoothness loss. This emphasizes depth consistency within the same semantic mask. The specific loss function is expressed as:

$$L_{mes}(D_t, I_t) = \sum M_i \left( |\partial_x D_t| e^{-|\partial_x I_t|} + |\partial_y D_t| e^{-|\partial_y I_t|} \right) \quad (6)$$

where  $M_i$  represents the auto-generated masks,  $\partial D_t$  and  $\partial I_t$  are the gradients of the depth map and image. Under mask guidance, the depth map is smoothed in non-edge regions while preserving gradients and details at the edges.

TABLE I  
THE CALCULATION OF APPLIED EVALUATION METRICS, IN WHICH  $d$  REPRESENTS THE PREDICTION DEPTH AND  $d^*$  REPRESENTS THE GROUND TRUTH.

Metric	Definition
Abs Rel	$\frac{1}{ N } \sum_{d \in N}  d - d^*  / d^*$
Sq Rel	$\frac{1}{ N } \sum_{d \in N}  d - d^* ^2 / d^*$
RMSE	$\sqrt{\frac{1}{ N } \sum_{d \in N} (d - d^*)^2}$
RMSE log	$\sqrt{\frac{1}{ N } \sum_{d \in N} (\ln d - \ln d^*)^2}$
$\delta_1, \delta_2$ , and $\delta_3$	$\frac{1}{ N } \sum [\max \left( \frac{d}{d^*}, \frac{d^*}{d} \right) < T], T \in \{1.25, 1.25^2, 1.25^3\}$

Integrating the various modules discussed above, the final loss function is defined as:

$$loss = \lambda_{ds} L_{ds} + \lambda_a L_a + \lambda_{ms} L_{ms} + \lambda_{mes} L_{mes} \quad (7)$$

where  $L_{ds}$ ,  $L_a$ ,  $L_{ms}$ , and  $L_{mes}$  are weighting factors. All modules are trained end-to-end using self-supervised objectives, including decomposing-synthesis loss, reflectance consistency loss, mapping-synthesis loss, and the proposed mask-guided smoothness loss.

## IV. EXPERIMENT

### A. Datasets and metrics

Our experiments are conducted on four publicly available datasets: SCARED [33], Hamlyn [34], SERV-CT [35], and EndoNeRF [36]. We perform training and test on the SCARED and Hamlyn datasets, and directly apply the trained network on the SCARED to the SERV-CT and EndoNeRF datasets to further validate the advantage of the proposed method.

SCARED dataset, originating from the 2019 MICCAI challenge, comprises nine subsets collected from porcine cadavers using the da Vinci surgical robot. Each subset contains 4 to 5 stereo video sequences, with ground truth depth maps obtained using structured light encoding during the acquisition process. For monocular depth estimation, as in previous works [7], [9], we only use the left-view images which are uniformly resized to  $320 \times 256$ . The dataset is divided into 15,351 frames for training, 1,705 frames for validation, and 551 frames for testing.

Hamlyn dataset is an in vivo endoscopy stereo video dataset provided by the Hamlyn Center for Laparoscopy at Imperial College London. We adopted the rectified version provided by Recasens et al. [37], along with the ground truth depth maps for left-view frames. The image size is  $288 \times 256$ , with 12,796 frames allocated for training, 2,076 for validation, and 2,319 for testing.

SERV-CT dataset consists of 16 endoscopic stereo image pairs captured using the da Vinci surgical robot on two different ex vivo porcine samples. Depth maps for the endoscopic images were computed by precisely aligning 3D models derived from CT images with the endoscopic stereo images. The test dataset contains a total of 32 frames, each with a resolution of  $720 \times 576$ .

EndoNeRF dataset includes two endoscopic scenes generated by the da Vinci surgical robot, depicting "cutting tissues

TABLE II

COMPARATIVE EXPERIMENTAL RESULTS ON THE SCARED DATASET AND PARAMETER COUNTS OF DIFFERENT METHODS. THE BEST RESULTS ARE PRESENTED IN BOLD.

Method	Abs Rel $\downarrow$	Sq Rel $\downarrow$	RMSE $\downarrow$	RMSE log $\downarrow$	$\delta 1 \uparrow$	$\delta 2 \uparrow$	$\delta 3 \uparrow$	Total.(M)	Train.(M)
Monodepth2 [8]	0.065	0.560	5.682	0.092	0.959	0.996	0.999	14.84	14.84
AF-SfMLearner [9]	0.064	0.536	5.545	0.089	0.964	0.996	0.999	14.84	14.84
IID-SfMLearner [7]	0.058	0.430	4.808	0.080	0.972	0.998	0.999	14.84	14.84
MonoPCC [13]	0.053	0.368	4.616	0.075	0.981	0.998	<b>1.000</b>	-	-
Depth Anything [5]	0.086	0.927	6.956	0.112	0.929	0.993	0.999	97.50	97.50
EndoDAC [19]	0.054	0.382	4.655	0.076	0.976	0.998	<b>1.000</b>	99.09	1.66
Ours	<b>0.050</b>	<b>0.317</b>	<b>4.141</b>	<b>0.070</b>	<b>0.982</b>	<b>0.999</b>	<b>1.000</b>	99.10	1.67

TABLE III

COMPARATIVE EXPERIMENTAL RESULTS ON HAMLYN DATASET. THE BEST RESULTS ARE PRESENTED IN BOLD.

Method	Abs Rel $\downarrow$	Sq Rel $\downarrow$	RMSE $\downarrow$	RMSE log $\downarrow$	$\delta 1 \uparrow$	$\delta 2 \uparrow$	$\delta 3 \uparrow$
Monodepth2 [8]	0.094	0.718	5.566	0.118	0.921	0.997	0.999
AF-SfMLearner [9]	0.087	0.656	5.134	0.108	0.925	<b>0.998</b>	<b>0.999</b>
IID-SfMLearner [7]	0.085	0.619	5.055	0.106	0.936	<b>0.998</b>	<b>0.999</b>
MonoPCC [13]	0.083	0.550	4.942	0.106	0.959	0.997	<b>0.999</b>
Depth Anything [5]	0.099	0.979	6.193	0.125	0.901	0.989	0.998
EndoDAC [19]	0.088	0.666	5.203	0.109	0.929	<b>0.998</b>	<b>0.999</b>
Ours	<b>0.071</b>	<b>0.445</b>	<b>4.280</b>	<b>0.089</b>	<b>0.973</b>	<b>0.998</b>	<b>0.999</b>

“twice” and “pulling soft tissues.” Each image has a resolution of  $640 \times 512$  and is accompanied by corresponding depth maps and surgical tool masks. The stereo depth maps are obtained using STTR-Light [38], and the tool masks are extracted manually. As with the previous datasets, we use 219 left-view images for testing.

We employ seven commonly used metrics in the evaluation, i.e., Abs Rel, Sq Rel, RMSE, RMSE log, and Threshold  $\delta 1$ ,  $\delta 2$ ,  $\delta 3$ , which are listed in Table I. Same with other methods [4], [9], we scale the predicted depth map due to its unknown scale. The scaling factor is the ground truth median depth divided by the predicted median depth, which can be expressed as:

$$f_{scale} = \text{median}(d^*)/\text{median}(d) \quad (8)$$

where  $d$  represents the prediction depth, and  $d^*$  represents the ground truth. The scaled depth map is capped at 150 mm for all the datasets, which can cover all pixels.

To evaluate camera pose estimation performance, we align the predicted camera trajectory to the scale of the ground-truth trajectory and employ the Absolute Trajectory Error (ATE) metric computed over 5-frame segments as the evaluation metric.

### B. Implementation details

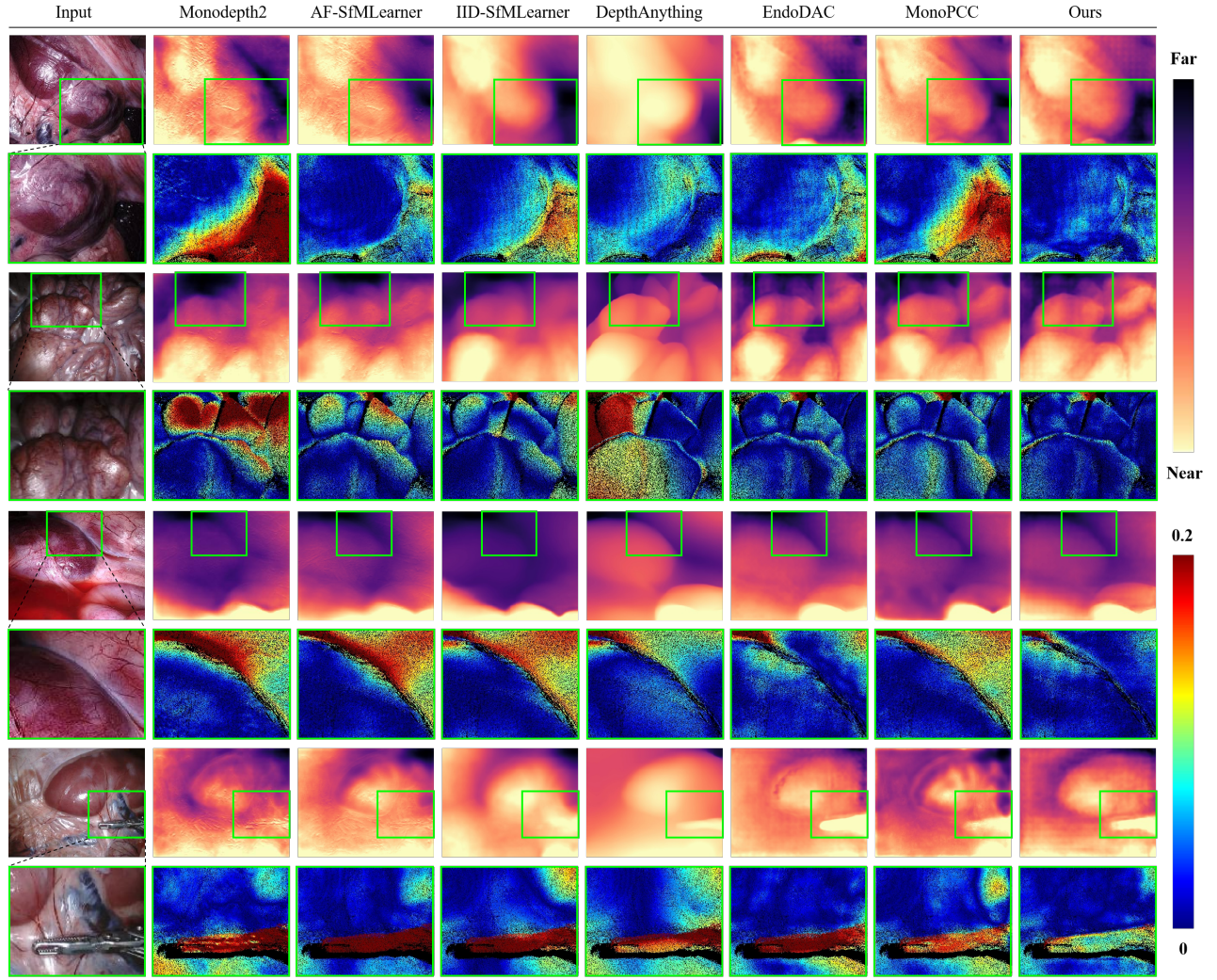
We train all the models end-to-end using PyTorch [39] and the Adam optimizer [40] with  $\beta_1 = 0.9$  and  $\beta_2 = 0.999$ . Our model is trained for 30 epochs on a GeForce A100 GPU with a batch size of 8. For training on the SCARED dataset, the initial learning rate is set to  $1 \times 10^{-4}$  and is multiplied by a scale factor of 0.1 after 10 epochs. In our experiments, the rank for RVLORA is set to 4, the loss weights  $L_{ds}$ ,  $L_a$ ,  $L_{ms}$  and  $L_{mes}$  are set to 0.2, 0.2, 1, and 0.003, respectively. When training on the Hamlyn dataset, the initial learning

rate is adjusted to  $5 \times 10^{-5}$ , and  $L_{mes}$  is set to 0.006. All other hyperparameters remain consistent with the SCARED dataset training.

### C. Comparison Experiments

We compare our method with six leading unsupervised monocular depth estimation methods, i.e., Monodepth2 [8], AF-SfMLearner [9], IID-SfMLearner [7], Depth Anything [5], EndoDAC [19], and MonoPCC [13]. The first three methods and EndoDAC were retrained using their publicly released codes, the methods Depth Anything and MonoPCC were tested using the trained model provided by the authors. Their performance was compared with that of our proposed method on the same test dataset.

The quantitative results on the SCARED dataset, detailed in Table II, demonstrate the superiority of our EndoUFM framework. Our model achieves state-of-the-art performance across all seven evaluation metrics. Earlier methods like Monodepth2, designed for natural images, struggle with the unique challenges of endoscopic scenes, such as variable lighting and specular reflections. While AF-SfMLearner and IID-SfMLearner introduced mechanisms to handle illumination inconsistencies, and MonoPCC utilized frequency domain information to achieve better results, our method surpasses them all. The direct application of the Depth Anything model, pre-trained on natural images, yields suboptimal results due to the significant domain gap. EndoDAC, which represents an initial effort in fine-tuning foundation models for endoscopy, shows improved performance. However, our method, with its more sophisticated integration of dual foundation models and advanced fine-tuning strategy, sets a new benchmark. Notably, EndoUFM reduces the Sq Rel by 9.17% compared to MonoPCC and 17.02% compared to EndoDAC, and it lowers the RMSE by 7.73% and 11.04%



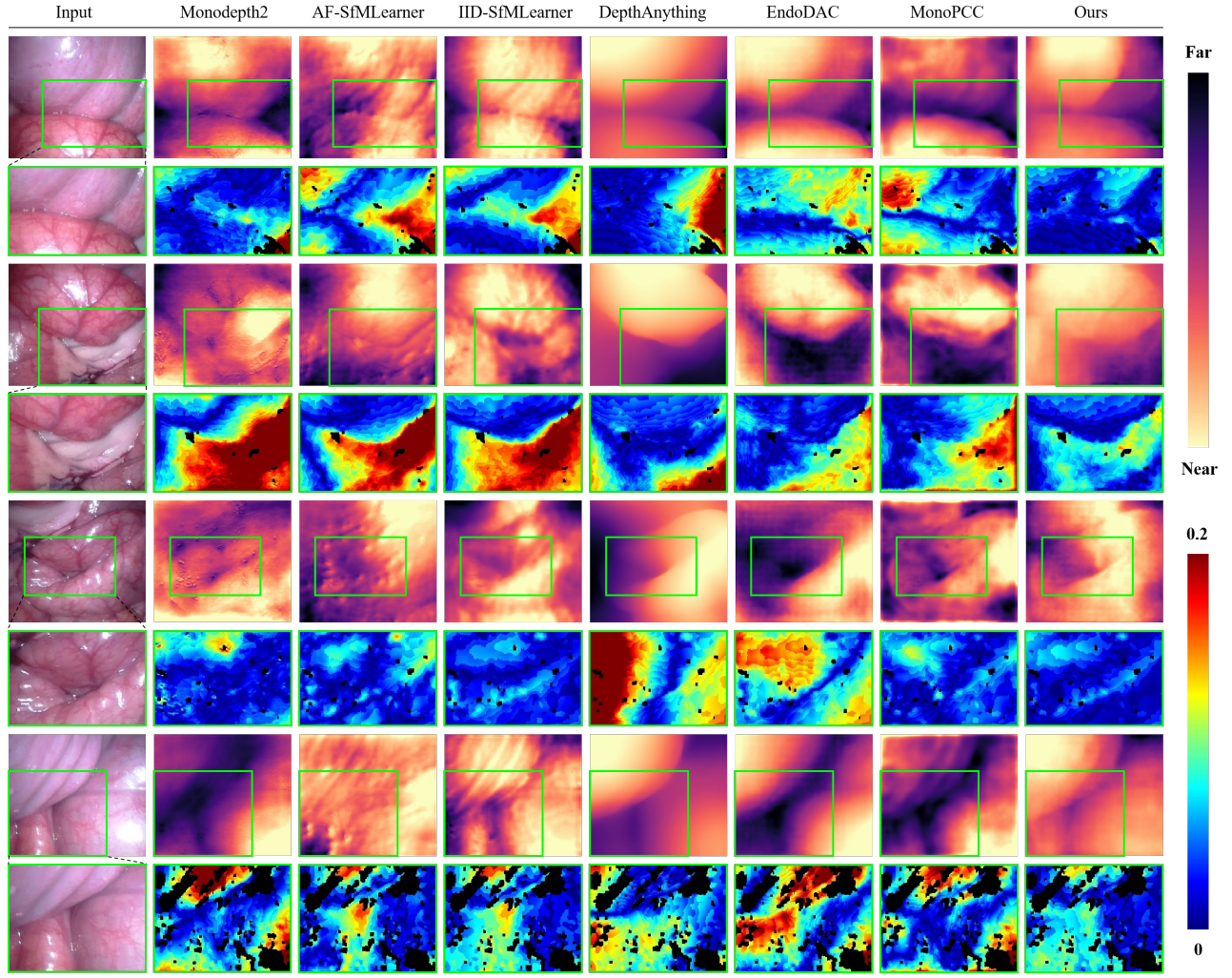


TABLE IV  
COMPARATIVE EXPERIMENTAL RESULTS ON SERV-CT DATASET. THE BEST RESULTS ARE PRESENTED IN BOLD.

Method	Abs Rel $\downarrow$	Sq Rel $\downarrow$	RMSE $\downarrow$	RMSE log $\downarrow$	$\delta 1 \uparrow$	$\delta 2 \uparrow$	$\delta 3 \uparrow$
Monodepth2 [8]	0.149	3.808	17.361	0.200	0.736	0.936	0.993
AF-SfMLearner [9]	0.124	2.233	13.125	0.155	0.845	0.985	1.000
IID-SfMLearner [7]	0.138	1.762	9.054	0.166	0.805	0.988	1.000
MonoPCC [13]	0.089	1.141	9.527	0.113	0.927	<b>0.999</b>	<b>1.000</b>
Depth Anything [5]	0.125	2.984	13.163	0.145	0.850	0.970	0.995
EndoDAC [19]	0.082	1.088	9.208	0.109	0.934	0.998	<b>1.000</b>
Ours	<b>0.071</b>	<b>0.791</b>	<b>8.025</b>	<b>0.092</b>	<b>0.965</b>	<b>0.999</b>	<b>1.000</b>

TABLE V  
COMPARATIVE EXPERIMENTAL RESULTS ON ENDONERF DATASET. THE BEST RESULTS ARE PRESENTED IN BOLD.

Method	Abs Rel $\downarrow$	Sq Rel $\downarrow$	RMSE $\downarrow$	RMSE log $\downarrow$	$\delta 1 \uparrow$	$\delta 2 \uparrow$	$\delta 3 \uparrow$
Monodepth2 [8]	0.223	5.484	19.417	0.278	0.543	0.885	0.993
AF-SfMLearner [9]	0.249	6.898	21.388	0.308	0.571	0.815	0.971
IID-SfMLearner [7]	0.225	5.760	19.958	0.286	0.542	0.881	0.994
MonoPCC [13]	0.210	5.070	19.250	0.274	0.547	0.891	0.995
Depth Anything [5]	0.230	5.669	21.061	0.266	0.504	0.923	0.995
EndoDAC [19]	<b>0.161</b>	3.017	16.061	<b>0.203</b>	0.725	0.974	<b>0.998</b>
Ours	0.163	<b>2.926</b>	<b>15.818</b>	0.207	<b>0.728</b>	<b>0.976</b>	0.997

TABLE VI  
THE ABLATION STUDY RESULTS OF THE PROPOSED MODULES.

Pre-trained	DepthAnything			SegmentAnything			$L_{mes}$	Metrics						
	RVLoRA	Res-DSC		Pre-trained	RVLoRA	Res-DSC		Abs Rel $\downarrow$	Sq Rel $\downarrow$	RMSE $\downarrow$	RMSE log $\downarrow$	$\delta 1 \uparrow$	$\delta 2 \uparrow$	$\delta 3 \uparrow$
✗	✗	✗		✗	✗	✗	✗	0.058	0.430	4.808	0.080	0.972	0.998	0.999
✓	✗	✗		✗	✗	✗	✗	0.085	0.915	7.182	0.116	0.936	0.991	0.996
✓	✓	✗		✗	✗	✗	✗	0.052	0.352	4.363	0.072	0.979	0.998	<b>1.000</b>
✓	✓	✓	✓	✗	✗	✗	✗	0.051	0.335	4.305	0.071	<b>0.982</b>	0.998	<b>1.000</b>
✓	✓	✓	✓	✓	✗	✗	✗	0.055	0.383	4.561	0.077	0.972	0.998	<b>1.000</b>
✓	✓	✓	✓	✓	✓	✗	✗	0.051	0.329	4.199	<b>0.070</b>	0.981	0.998	<b>1.000</b>
✓	✓	✓	✓	✓	✓	✓	✗	0.055	0.414	4.742	0.077	0.975	0.997	<b>1.000</b>
✓	✓	✓	✓	✓	✓	✗	✓	<b>0.050</b>	<b>0.317</b>	<b>4.141</b>	<b>0.070</b>	<b>0.982</b>	<b>0.999</b>	<b>1.000</b>

TABLE VII  
THE COMPARISON OF LORA METHODS AND VECTOR INITIALIZATION.

	Abs Rel $\downarrow$	Sq Rel $\downarrow$	RMSE $\downarrow$	RMSE log $\downarrow$	$\delta 1 \uparrow$	$\delta 2 \uparrow$	$\delta 3 \uparrow$	
LoRA methods	LoRA [12]	<b>0.050</b>	0.321	4.182	<b>0.070</b>	0.980	0.998	<b>1.000</b>
	VeRA [24]	0.056	0.414	4.726	0.078	0.972	0.997	0.999
	DV-LoRA [19]	0.052	0.346	4.301	0.072	0.980	0.998	<b>1.000</b>
	RVLoRA(Ours)	<b>0.050</b>	<b>0.317</b>	<b>4.141</b>	<b>0.070</b>	<b>0.982</b>	<b>0.999</b>	<b>1.000</b>
$a, b$ Init.	Uniform	0.054	0.395	4.634	0.076	0.979	0.997	<b>1.000</b>
	Kaiming Normal	0.052	0.349	4.336	0.073	0.975	0.998	<b>1.000</b>
	Kaiming Uniform(Ours)	<b>0.050</b>	<b>0.317</b>	<b>4.141</b>	<b>0.070</b>	<b>0.982</b>	<b>0.999</b>	<b>1.000</b>

TABLE VIII  
THE RESULTS OF POSE ESTIMATION.

Method	ATE (Seq 1) $\downarrow$	ATE (Seq 2) $\downarrow$	ATE (Seq 3) $\downarrow$
AF-SfMLearner [9]	0.0440	0.0558	0.0544
MonoPCC [13]	0.0596	0.0617	0.0825
EndoDAC [19]	0.0439	0.0577	0.0529
Ours	<b>0.0424</b>	<b>0.0537</b>	<b>0.0516</b>

frozen scaling parameters.

### E. Pose Estimation

We evaluate the self-motion estimation performance of our method against other approaches using three image sequences from the SCARED dataset. Table VIII presents

the quantitative comparison results with highly competitive methods, AF-SfMLearner, MonoPCC, and EndoDAC. Our method achieves optimal performance across all three sequences, demonstrating an average reduction of 3.21% compared to the next best result.

Fig. 6 illustrates the predicted trajectories for three sequences from different methods, with all trajectories aligned at their starting points. Our method's trajectory is consistently the closest to the ground truth (represented by the black curve), exhibiting minimal trajectory drift. This demonstrates the superior performance of our approach in pose estimation.

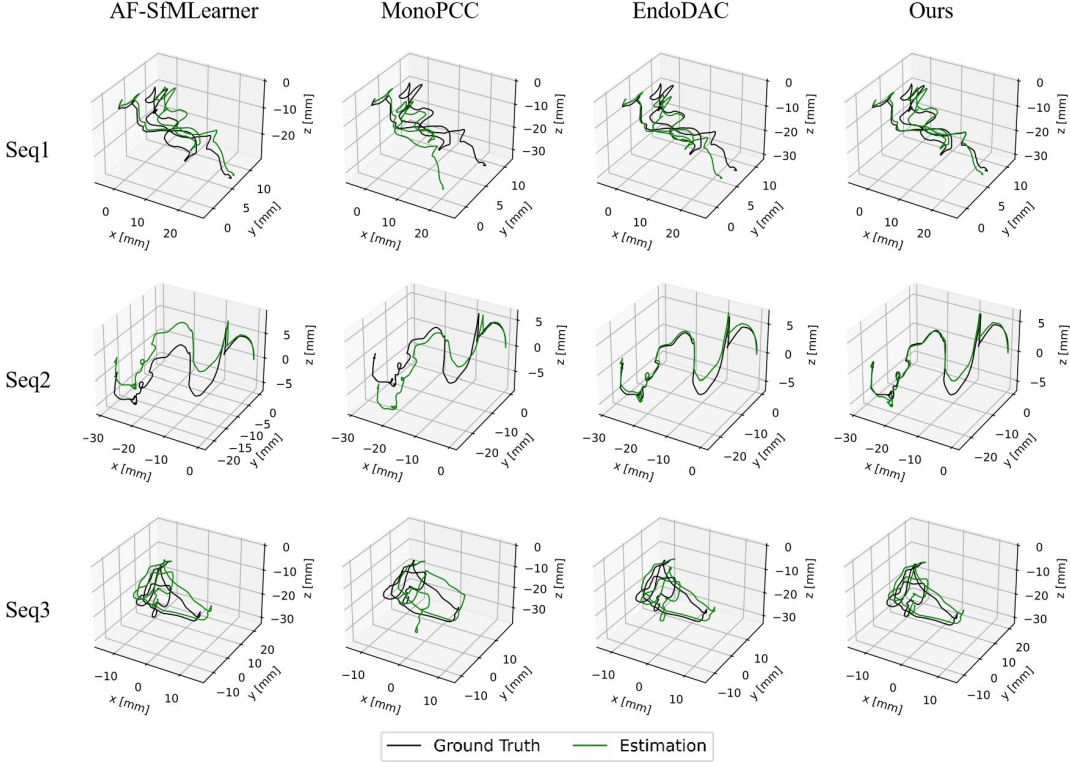


Fig. 6. Visualization of camera pose estimation trajectories on the SCARED dataset. The black curve represents the ground truth trajectory. The green curves show the estimated trajectories from different methods.

## V. DISCUSSION AND CONCLUSION

Self-supervised monocular depth estimation for endoscopic images remains challenging due to varying illumination and complex tissue textures. In this work, we introduce EndoUFM, a novel self-supervised framework that utilizes foundation models to enhance depth estimation accuracy, robustness, and generalization. Specifically, our method leverages large-scale, pre-learned knowledge by integrating priors from the Depth Anything Model and the Segment Anything Model. This provided a robust foundation for understanding the complex structures within the surgical scene. To emphasize model adaptability and the capture of fine-grained features, we design an adaptive fine-tuning strategy for foundation models, combining RV-LoRA and Res-DSC. Furthermore, we introduce a mask-guided smoothness loss based on pre-segmented masks, which effectively mitigates semantic ambiguities in depth predictions. Extensive experiments on four benchmark datasets demonstrate that our method achieves state-of-the-art performance, surpassing existing approaches and exhibiting exceptional robustness in challenging scenarios. Ablation studies are designed to validate the efficacy of the foundation models utilization and proposed adaptive fine-tuning strategy. Finally, we evaluate and visualize the camera pose estimation results, further demonstrating the effectiveness of our approach. Despite the excellent performance, our method still exhibits some limitations in areas with uneven illumination or low brightness. Therefore, we plan to incorporate 3D scene perception in

future work to mitigate the impact of lighting variations on depth estimation performance.

In conclusion, the EndoUFM framework establishes a new state-of-the-art in unsupervised monocular depth estimation for endoscopic scenes. Beyond its current applications, this approach can be further explored for its ability to provide reliable point cloud initialization, opening avenues for subsequent 3D reconstruction using methods like NeRF [41] and 3D Gaussian Splatting [42]. Ultimately, these advancements are a crucial step toward creating more sophisticated Augmented Reality (AR) and surgical navigation systems, with the potential to significantly enhance procedural precision and safety in Minimally Invasive Surgery.

## REFERENCES

- [1] A. K. Sharma, R. G. de Oliveira, S. Suvithayasiri, P. Chavalparit, C. C. Chang, Y. H. Kim, C. R. Fischer, S. Lee, S. Cho, J.-S. Kim, *et al.*, “The utilization of navigation and emerging technologies with endoscopic spine surgery: A narrative review,” *Neurospine*, vol. 22, no. 1, p. 105, 2025.
- [2] Z. Yang, J. Pan, J. Dai, Z. Sun, and Y. Xiao, “Self-supervised lightweight depth estimation in endoscopy combining cnn and transformer,” *IEEE Transactions on Medical Imaging*, vol. 43, no. 5, pp. 1934–1944, 2024.
- [3] Z. Liu, C. Song, J. Cheng, J. Luo, and X. Wang, “Self-supervised monocular depth estimation with effective feature fusion and self distillation,” in *2024 IEEE/RSJ International Conference on Intelligent Robots and Systems (IROS)*, pp. 7160–7166, IEEE, 2024.
- [4] T. Zhou, M. Brown, N. Snavely, and D. G. Lowe, “Unsupervised learning of depth and ego-motion from video,” in *Proceedings of the IEEE conference on computer vision and pattern recognition*, pp. 1851–1858, 2017.

[5] L. Yang, B. Kang, Z. Huang, X. Xu, J. Feng, and H. Zhao, "Depth anything: Unleashing the power of large-scale unlabeled data," in *Proceedings of the IEEE/CVF conference on computer vision and pattern recognition*, pp. 10371–10381, 2024.

[6] K. B. Ozyoruk, G. I. Gokceler, T. L. Bobrow, G. Coskun, K. Incetan, Y. Almalioglu, F. Mahmood, E. Curto, L. Perdigoto, M. Oliveira, *et al.*, "Endoslam dataset and an unsupervised monocular visual odometry and depth estimation approach for endoscopic videos," *Medical image analysis*, vol. 71, p. 102058, 2021.

[7] B. Li, B. Liu, M. Zhu, X. Luo, and F. Zhou, "Image intrinsic-based unsupervised monocular depth estimation in endoscopy," *IEEE Journal of Biomedical and Health Informatics*, 2024.

[8] C. Godard, O. Mac Aodha, M. Firman, and G. J. Brostow, "Digging into self-supervised monocular depth estimation," in *Proceedings of the IEEE/CVF international conference on computer vision*, pp. 3828–3838, 2019.

[9] S. Shao, Z. Pei, W. Chen, W. Zhu, X. Wu, D. Sun, and B. Zhang, "Self-supervised monocular depth and ego-motion estimation in endoscopy: Appearance flow to the rescue," *Medical image analysis*, vol. 77, p. 102338, 2022.

[10] J. J. Han, A. Acar, C. Henry, and J. Y. Wu, "Depth anything in medical images: A comparative study," *arXiv preprint arXiv:2401.16600*, 2024.

[11] J. Ma, Y. He, F. Li, L. Han, C. You, and B. Wang, "Segment anything in medical images," *Nature Communications*, vol. 15, no. 1, p. 654, 2024.

[12] E. J. Hu, yelong shen, P. Wallis, Z. Allen-Zhu, Y. Li, S. Wang, L. Wang, and W. Chen, "LoRA: Low-rank adaptation of large language models," in *International Conference on Learning Representations*, 2022.

[13] Z. Wang, Y. Zhou, S. He, T. Li, F. Huang, Q. Ding, X. Feng, M. Liu, and Q. Li, "Monopcc: Photometric-invariant cycle constraint for monocular depth estimation of endoscopic images," *Medical Image Analysis*, vol. 102, p. 103534, 2025.

[14] V. M. Battile, J. M. Montiel, and J. D. Tardós, "Photometric single-view dense 3d reconstruction in endoscopy," in *2022 IEEE/RSJ International Conference on Intelligent Robots and Systems (IROS)*, pp. 4904–4910, IEEE, 2022.

[15] R. Ranftl, K. Lasinger, D. Hafner, K. Schindler, and V. Koltun, "Towards robust monocular depth estimation: Mixing datasets for zero-shot cross-dataset transfer," *IEEE transactions on pattern analysis and machine intelligence*, vol. 44, no. 3, pp. 1623–1637, 2020.

[16] M. Oquab, T. Dariseti, T. Moutakanni, H. Vo, M. Szafrańiec, V. Khalidov, P. Fernandez, D. Haziza, F. Massa, A. El-Nouby, *et al.*, "Dinov2: Learning robust visual features without supervision," *Transactions on Machine Learning Research Journal*, pp. 1–31, 2024.

[17] Q. Tian, Z. Chen, H. Liao, X. Huang, L. Li, S. Ourselin, and H. Liu, "Endoomni: Zero-shot cross-dataset depth estimation in endoscopy by robust self-learning from noisy labels," *arXiv preprint arXiv:2409.05442*, 2024.

[18] B. Cui, M. Islam, L. Bai, and H. Ren, "Surgical-dino: adapter learning of foundation models for depth estimation in endoscopic surgery," *International Journal of Computer Assisted Radiology and Surgery*, vol. 19, no. 6, pp. 1013–1020, 2024.

[19] B. Cui, M. Islam, L. Bai, A. Wang, and H. Ren, "Endodac: Efficient adapting foundation model for self-supervised depth estimation from any endoscopic camera," in *International Conference on Medical Image Computing and Computer-Assisted Intervention*, pp. 208–218, Springer, 2024.

[20] Z. Yang, J. Pan, J. Dai, Z. Sun, and Y. Xiao, "Self-supervised endoscopy depth estimation framework with clip-guidance segmentation," *Biomedical Signal Processing and Control*, vol. 95, p. 106410, 2024.

[21] A. Radford, J. W. Kim, C. Hallacy, A. Ramesh, G. Goh, S. Agarwal, G. Sastry, A. Askell, P. Mishkin, J. Clark, *et al.*, "Learning transferable visual models from natural language supervision," in *International conference on machine learning*, pp. 8748–8763, PMLR, 2021.

[22] S. Hayou, N. Ghosh, and B. Yu, "Lora+: Efficient low rank adaptation of large models," in *International Conference on Machine Learning*, pp. 17783–17806, PMLR, 2024.

[23] Q. Zhang, M. Chen, A. Bukharin, P. He, Y. Cheng, W. Chen, and T. Zhao, "Adaptive budget allocation for parameter-efficient fine-tuning," in *11th International Conference on Learning Representations, ICLR 2023*, 2023.

[24] D. J. Kopiczko, T. Blankevoort, and Y. M. Asano, "VeRA: Vector-based random matrix adaptation," in *12th International Conference on Learning Representations*, 2024.

[25] A. Kirillov, E. Mintun, N. Ravi, H. Mao, C. Rolland, L. Gustafson, T. Xiao, S. Whitehead, A. C. Berg, W.-Y. Lo, *et al.*, "Segment anything," in *Proceedings of the IEEE/CVF international conference on computer vision*, pp. 4015–4026, 2023.

[26] A. Aghajanyan, S. Gupta, and L. Zettlemoyer, "Intrinsic dimensionality explains the effectiveness of language model fine-tuning," in *Proceedings of the 59th Annual Meeting of the Association for Computational Linguistics and the 11th International Joint Conference on Natural Language Processing (Volume 1: Long Papers)*, pp. 7319–7328, 2021.

[27] K. Lu, A. Grover, P. Abbeel, and I. Mordatch, "Frozen pretrained transformers as universal computation engines," in *Proceedings of the AAAI conference on artificial intelligence*, vol. 36, pp. 7628–7636, 2022.

[28] J. Frankle, D. J. Schwab, and A. S. Morcos, "Training batchnorm and only batchnorm: On the expressive power of random features in {cnn}s," in *International Conference on Learning Representations*, 2021.

[29] K. He, X. Zhang, S. Ren, and J. Sun, "Delving deep into rectifiers: Surpassing human-level performance on imagenet classification," in *Proceedings of the IEEE international conference on computer vision*, pp. 1026–1034, 2015.

[30] M. Shvets, D. Zhao, M. Niethammer, R. Sengupta, and A. C. Berg, "Joint depth prediction and semantic segmentation with multi-view sam," in *Proceedings of the IEEE/CVF Winter Conference on Applications of Computer Vision*, pp. 1328–1338, 2024.

[31] S. Woo, J. Park, J.-Y. Lee, and I. S. Kweon, "Cbam: Convolutional block attention module," in *Proceedings of the European conference on computer vision (ECCV)*, pp. 3–19, 2018.

[32] A. Krebs, Y. Benzeth, and F. Marzani, "Intrinsic image decomposition as two independent deconvolution problems," *Signal Processing: Image Communication*, vol. 86, p. 115872, 2020.

[33] M. Allan, J. Mcleod, C. Wang, J. C. Rosenthal, Z. Hu, N. Gard, P. Eisert, K. X. Fu, T. Zeffiro, W. Xia, *et al.*, "Stereo correspondence and reconstruction of endoscopic data challenge," *arXiv preprint arXiv:2101.01133*, 2021.

[34] P. Mountney, D. Stoyanov, and G.-Z. Yang, "Three-dimensional tissue deformation recovery and tracking," *IEEE Signal Processing Magazine*, vol. 27, no. 4, pp. 14–24, 2010.

[35] P. E. Edwards, D. Psychogios, S. Speidel, L. Maier-Hein, and D. Stoyanov, "Serv-ct: A disparity dataset from cone-beam ct for validation of endoscopic 3d reconstruction," *Medical image analysis*, vol. 76, p. 102302, 2022.

[36] Y. Wang, Y. Long, S. H. Fan, and Q. Dou, "Neural rendering for stereo 3d reconstruction of deformable tissues in robotic surgery," in *International conference on medical image computing and computer-assisted intervention*, pp. 431–441, Springer, 2022.

[37] D. Recasens, J. Lamarca, J. M. Fácil, J. M. Montiel, and J. Civera, "Endo-depth-and-motion: Reconstruction and tracking in endoscopic videos using depth networks and photometric constraints," *IEEE Robotics and Automation Letters*, vol. 6, no. 4, pp. 7225–7232, 2021.

[38] Z. Li, X. Liu, N. Drenkow, A. Ding, F. X. Creighton, R. H. Taylor, and M. Unberath, "Revisiting stereo depth estimation from a sequence-to-sequence perspective with transformers," in *Proceedings of the IEEE/CVF international conference on computer vision*, pp. 6197–6206, 2021.

[39] A. Paszke, S. Gross, F. Massa, A. Lerer, J. Bradbury, G. Chanan, T. Killeen, Z. Lin, N. Gimelshein, L. Antiga, *et al.*, "Pytorch: An imperative style, high-performance deep learning library," *Advances in neural information processing systems*, vol. 32, 2019.

[40] D. P. Kingma and J. Ba, "Adam: A method for stochastic optimization," in *3rd International Conference on Learning Representations, ICLR 2015, Conference Track Proceedings*, 2015.

[41] B. Mildenhall, P. P. Srinivasan, M. Tancik, J. T. Barron, R. Ramamoorthi, and R. Ng, "Nerf: Representing scenes as neural radiance fields for view synthesis," *Communications of the ACM*, vol. 65, no. 1, pp. 99–106, 2021.

[42] B. Kerbl, G. Kopanas, T. Leimkühler, and G. Drettakis, "3d gaussian splatting for real-time radiance field rendering," *ACM Transactions on Graphics*, vol. 42, no. 4, pp. 1–14, 2023.